Data-Driven Adaptive Negative Sequence Current Control Method for PWM Rectifier Under Unbalanced Grid

Tianbao Song, Yun Zhang, *Senior Member, IEEE*, Fei Gao, *Member, IEEE*, Chengqian Xu, and Xinshan Zhu, *Member, IEEE*

***Abstract*—Three phase pulse width modulation (PWM) rectifiers have excellent performance when the grid voltages are balanced, and it is widely adopted in the industry. However, the asymmetrical loads or grid faults will lead to the unbalanced grid voltages. In addition, the negative sequence (NS) voltages and currents in the unbalanced grid result in the fluctuation of the dc bus voltage. In this article, the intrinsic mechanism between the voltage ripple amplitude and the NS currents is revealed. Furthermore, this article proposes a data-driven adaptive current control method. By shaping the NS currents, the corresponding amplitudes of the second-order harmonic voltage on the dc bus are observed. Based on the observation data, the reference currents that can minimize the dc bus voltage ripple are adaptively derived online. As a result, the dc bus voltage ripple can be suppressed effectively. In addition, the proposed method does not need the NS decomposition or the parameters such as the grid voltages and inductances. Therefore, it has a strong robustness against parameter mismatch. Finally, the accuracy of the theoretical analysis and the effectiveness of the proposed method are validated by experiments.**

***Index Terms*—Data-driven, dc bus voltage ripple, negative sequence current control, three-phase pulse width modulation (PWM) rectifier, unbalanced grid.**

I. Introduction

THREE-PHASE pulse width modulation (PWM) rectifiers can achieve a bidirectional power flow, a high-power factor, and a low current harmonic rectification [1], [2]. As a result, it has excellent performance under balanced grid conditions. Hence, three-phase PWM rectifiers have wide applications in motor drives [3], high-voltage dc power transmissions [4], and microgrids [5], [6]. Besides, with the rapid growth of electric vehicles (EVs) ownership, the three-phase PWM rectifiers also play an important role in EV charging systems [7], [8]. However, the unbalanced grid often occurs, due to the increasing penetration of the renewable energy sources, and unbalanced grid loads [9].

Since the unbalanced grid voltages contain negative sequence (NS) components, there are ac components in the output power that results in the ac component in the dc bus voltage [10]. When the EV is charging in this condition, the fluctuating dc voltage will cause problems, such as the battery heating and gassing, which can increase the unsafe factors [11], [12]. Concomitantly, the risk of power switching overvoltage will also be elevated [13]. In addition, the dc bus voltage ripple will increase the odd harmonics in grid currents, which poses challenge to the power quality. Therefore, literatures have been focused on the dc bus voltage ripple suppression under unbalanced grid [14].

Rioual et al. [15] established the positive and NS model of the three-phase PWM rectifier under unbalanced grid. Based on the model, a current compensation control method is proposed to improve the stability of system. However, the method does not essentially suppress the dc bus voltage pulsation, and the power quality still needs to be improved. In [16], the theoretical analysis and experimental research are conducted for voltage unbalance, phase loss, short circuit, and grounding faults, and an optimal modulation strategy is proposed to ensure the stable operation of the system under multiple faults. However, the issues on the dc bus voltage ripple and the grid current harmonics are not completely solved.

In recent years, a variety of flexible strategies to meet the multiple control objectives under unbalanced grid have been proposed. In [17], the coupling relationship between the second-order harmonic ripple of the dc bus voltage and the grid current harmonics is revealed. In addition, a grid current harmonic suppression method is proposed for the electric vehicle charging system. However, the method cannot suppress the dc bus voltage ripple, and the poststage dc–dc converter is required to buffer the pulsating voltage. As a result, this method has limited application scenarios. Guo et al. [18] proposed a flexible control strategy that can suppress either the dc bus voltage ripple or the grid current harmonics, which is simple and easy to implement. However, it cannot achieve the collaborative suppressions of the dc bus voltage ripple and the grid current harmonics. Thus, this method cannot be applied in situations where the high-power quality is required.

Manuscript received 10 May 2023; revised 11 September 2023 and 26 October 2023; accepted 2 January 2024. Date of publication 5 January 2024; date of current version 16 February 2024. This work was supported by the National Natural Science Foundation of China under Grant 51977145. Recommended for publication by Associate Editor C. Rim. *(Corresponding author: Yun Zhang.)*

Tianbao Song, Yun Zhang, Chengqian Xu, and Xinshan Zhu are with the School of Electrical and Information Engineering, Tianjin University, Tianjin 300072, China, and also with the National Industry-Education Platform of Energy Storage, Tianjin University, Tianjin 300072, China (e-mail: songtb@tju.edu.cn; zhangy@tju.edu.cn; xucq@tju.edu.cn; xszhu@tju.edu.cn).

Fei Gao is with the Department of Electrical Engineering, Shanghai Jiao Tong University, Shanghai 200240, China (e-mail: sjtugf@163.com).

Color versions of one or more figures in this article are available at https://doi.org/10.1109/TPEL.2024.3350205.

Digital Object Identifier 10.1109/TPEL.2024.3350205

To achieve the collaborative suppression of the dc bus voltage ripple and the grid current harmonics, Yin et al. [19] established a mathematical model of the output power under unbalanced grid conditions. In addition, the relationship between the output power pulsation and the rectifier voltage is given. Meanwhile, it is clarified that the dc bus voltage ripple suppression is essential to control the grid current asymmetry. By injecting the NS active and reactive currents, the output power ripple caused by the asymmetric voltage can be eliminated. According to [17], it is known that the grid current harmonics are caused by the dc bus voltage ripple. As a result, after eliminating the dc bus voltage ripple, the grid current harmonics can be indirectly suppressed. However, the output power control in [19] requires the positive and NS dual current loop controls, which increases the complexity of the system. Based on [19], the current is controlled in two-phase stationary coordinate, where the positive and NS currents can be added and controlled, respectively [20]. Thus, the dual current loops are not required, which effectively reduces the complexity of the system. Meanwhile, different control objectives are summarized, such as the input power control, the output power control, and the input–output power control, which lay a foundation for the subsequent research.

Based on the output power control, Zhang and Qu [21] and Zhang et al. [22] combined the direct power control (DPC) to eliminate the output power pulsation by superimposing the compensation on the power reference. In [23], the original and the delayed signals are employed instead of the positive and NS components. In addition, the feasibility of the method is experimentally verified. However, these methods are sensitive to the inductance. The control performance cannot be guaranteed when the inductance values are not accurate. Therefore, Zhang et al. [24] proposed a direct power control strategy with an online inductor identification, which improves the robustness to the inductance. However, the aforementioned methods still rely on the sampling and estimation of the grid and rectifier voltages. In [25], a voltage sensor-less direct power control method is proposed based on a sliding mode observer, which can effectively estimate the grid voltage by the current sampling. As a result, the dependence on voltage sampling can be profoundly reduced. However, this method still needs to estimate the grid and rectifier voltages, which requires the output power model.

In this article, a data-driven adaptive current control method is proposed. The main contributions are summarized as follows.

1) The intrinsic mechanism between the dc bus voltage ripple amplitude and the NS currents is revealed. In addition, the trend of the dc bus voltage ripple amplitude when the NS currents change is clarified.
2) A data-driven adaptive current control method is proposed. By shaping the NS currents and observing the amplitude of the dc bus voltage ripple, the NS reference currents that minimize the dc bus voltage ripple are solved. Therefore, the current reference calculation is upgraded from the model-driven mode to the data-driven one. Furthermore, the dc bus voltage ripple can be effectively suppressed with the strong robustness.
3) Since the grid voltages, inductance and capacitance are not required in the current reference calculation, control performance degradation due to the inaccurate mentioned parameters can be completely avoided. Hence, the robustness against parameter errors is achieved.

The rest of this article is organized as follows. Section II gives the mechanism of the dc bus voltage ripple generation. Section III proposes a data-driven adaptive current control method. Then, the experimental results and discussions are presented in Section IV. Finally, Section V concludes this article.

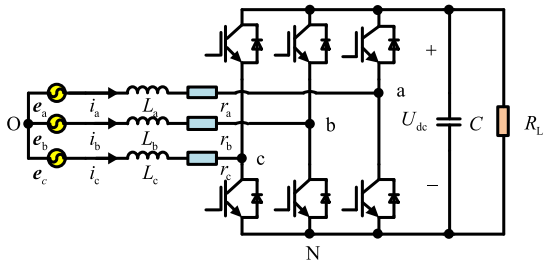

Fig. 1. Topology of the three-phase PWM rectifier.

II. DC Bus Voltage Ripple Under Unbalanced Grids

The topology of the three-phase PWM rectifier is shown in Fig. 1. The voltage equation of the PWM rectifier can be written as follows:

$$\boldsymbol{e}_x = \boldsymbol{v}_x + r_x \boldsymbol{i}_x + L_x \frac{\mathrm{d}\boldsymbol{i}_x}{\mathrm{d}t} \tag{1}$$

where x represents three-phase, a, b, and c. e, i, and v are the vectors of the grid voltage, the grid current, and the rectifier voltage, respectively. The filter inductance and its equivalent resistance in series are written as L and r, respectively.

When the grid unbalance occurs, the grid voltage, current and the rectifier voltage contain positive and NS component. Thus, the grid voltage $\boldsymbol{e}$ can be obtained as

$$\boldsymbol{e}_{\mathrm{dq}} = \boldsymbol{e}^{\mathrm{p}}_{\mathrm{dq}} \cdot e^{\mathrm{j}\omega_{\mathrm{f}} t} + \boldsymbol{e}^{\mathrm{n}}_{\mathrm{dq}} \cdot e^{-\mathrm{j}\omega_{\mathrm{f}} t} \tag{2}$$

where $\boldsymbol{e}^{\mathrm{p}}_{\mathrm{dq}} = e^{\mathrm{p}}_{\mathrm{d}} + \mathrm{j}e^{\mathrm{p}}_{\mathrm{q}}$ and $\boldsymbol{e}^{\mathrm{n}}_{\mathrm{dq}} = e^{\mathrm{n}}_{\mathrm{d}} + \mathrm{j}e^{\mathrm{n}}_{\mathrm{q}}$ are the positive and NS component of the grid voltage in d-q coordinate. Similarly, the grid current and rectifier voltage can be expressed as follows:

$$\begin{cases} \boldsymbol{i}_{\mathrm{dq}} = \boldsymbol{i}^{\mathrm{p}}_{\mathrm{dq}} \cdot e^{\mathrm{j}\omega_{\mathrm{f}} t} + \boldsymbol{i}^{\mathrm{n}}_{\mathrm{dq}} \cdot e^{-\mathrm{j}\omega_{\mathrm{f}} t} \\ \boldsymbol{v}_{\mathrm{dq}} = \boldsymbol{v}^{\mathrm{p}}_{\mathrm{dq}} \cdot e^{\mathrm{j}\omega_{\mathrm{f}} t} + \boldsymbol{v}^{\mathrm{n}}_{\mathrm{dq}} \cdot e^{-\mathrm{j}\omega_{\mathrm{f}} t}. \end{cases} \tag{3}$$

The NS components of the voltage and current lead to fluctuating output power. According to [21], the output power can be written as follows:

$$p^{\mathrm{out}} = P^{\mathrm{out}}_0 + P^{\mathrm{out}}_{\mathrm{c}} \cos(2\omega_{\mathrm{f}} t) + P^{\mathrm{out}}_{\mathrm{s}} \sin(2\omega_{\mathrm{f}} t) \tag{4}$$

$$\begin{bmatrix} P^{\mathrm{out}}_0 \\ P^{\mathrm{out}}_{\mathrm{c}} \\ P^{\mathrm{out}}_{\mathrm{s}} \end{bmatrix} = \frac{3}{2} \begin{bmatrix} v^{\mathrm{p}}_{\mathrm{d}} & v^{\mathrm{p}}_{\mathrm{q}} & v^{\mathrm{n}}_{\mathrm{d}} & v^{\mathrm{n}}_{\mathrm{q}} \\ v^{\mathrm{n}}_{\mathrm{d}} & v^{\mathrm{n}}_{\mathrm{q}} & v^{\mathrm{p}}_{\mathrm{d}} & v^{\mathrm{p}}_{\mathrm{q}} \\ v^{\mathrm{n}}_{\mathrm{q}} & -v^{\mathrm{n}}_{\mathrm{d}} & -v^{\mathrm{p}}_{\mathrm{q}} & v^{\mathrm{p}}_{\mathrm{d}} \end{bmatrix} \begin{bmatrix} i^{\mathrm{p}}_{\mathrm{d}} \\ i^{\mathrm{p}}_{\mathrm{q}} \\ i^{\mathrm{n}}_{\mathrm{d}} \\ i^{\mathrm{n}}_{\mathrm{q}} \end{bmatrix} \tag{5}$$

where p^{out} is the output active power, P^{out}_0 is the dc component of the output power, $P^{\mathrm{out}}_{\mathrm{c}}$ and $P^{\mathrm{out}}_{\mathrm{s}}$ are the sine and cosine ac components of the output power, respectively. ω_{f} is the fundamental angular frequency of the grid voltage.

In terms of (4), there are two ac components in the output power, and their angular frequency is $2\omega_{\mathrm{f}}$. As a result, the second-order harmonic voltage ripple exists the in the dc bus.

III. Proposed Data-Driven Adaptive Current Control Method

The dc bus voltage ripple leads to the grid current distortion, which will reduce the power quality of the PWM rectifier. In this section, a data-driven adaptive current control method is proposed and analyzed in detail.

A. Mechanism Between the DC Bus Voltage Ripple Amplitude and the NS Currents

Similar with the fluctuating output active power, the reactive power can be expressed as follows:

$$\begin{cases} Q_{\mathrm{c}}^{\mathrm{out}} = -\frac{3}{2}(v_{\mathrm{d}}^{\mathrm{n}} i_{\mathrm{d}}^{\mathrm{p}} + v_{\mathrm{q}}^{\mathrm{n}} i_{\mathrm{q}}^{\mathrm{p}} + v_{\mathrm{d}}^{\mathrm{p}} i_{\mathrm{d}}^{\mathrm{n}} + v_{\mathrm{q}}^{\mathrm{p}} i_{\mathrm{q}}^{\mathrm{n}}) \\ Q_{\mathrm{s}}^{\mathrm{out}} = \frac{3}{2}(v_{\mathrm{q}}^{\mathrm{n}} i_{\mathrm{d}}^{\mathrm{p}} - v_{\mathrm{d}}^{\mathrm{n}} i_{\mathrm{q}}^{\mathrm{p}} - v_{\mathrm{q}}^{\mathrm{p}} i_{\mathrm{d}}^{\mathrm{n}} + v_{\mathrm{d}}^{\mathrm{p}} i_{\mathrm{q}}^{\mathrm{n}}). \end{cases} \tag{6}$$

According to the conservation of reactive power, (7) can be written as follows:

$$Q_{\mathrm{c}}^{\mathrm{out}} \cos(2\omega_{\mathrm{f}} t) + Q_{\mathrm{s}}^{\mathrm{out}} \sin(2\omega_{\mathrm{f}} t) = C \frac{\mathrm{d}U_{\mathrm{dc}}}{\mathrm{d}t} U_{\mathrm{dc}}. \tag{7}$$

Furthermore, the left side of (7) can be written as follows:

$$\begin{aligned} &Q_{\mathrm{c}}^{\mathrm{out}} \cos(2\omega_{\mathrm{f}} t) + Q_{\mathrm{s}}^{\mathrm{out}} \sin(2\omega_{\mathrm{f}} t) \\ &= \sqrt{Q_{\mathrm{c}}^{\mathrm{out}\,2} + Q_{\mathrm{s}}^{\mathrm{out}\,2}} \sin\left(2\omega_{\mathrm{f}} t + \arctan\left(\frac{Q_{\mathrm{c}}^{\mathrm{out}}}{Q_{\mathrm{s}}^{\mathrm{out}}}\right)\right). \end{aligned} \tag{8}$$

Moreover, according to the analysis in Section II, the dc bus voltage contains an ac component with an angular frequency of 2 ω_{f}. Assuming that the ac and dc components of the dc bus voltage are $U_{\mathrm{dc\_ac}}$ and $U_{\mathrm{dc\_dc}}$, respectively, then the dc bus voltage can be written as follows:

$$U_{\mathrm{dc}} = U_{\mathrm{dc\_ac}} \sin(2\omega_{\mathrm{f}} t + \varphi_{u\mathrm{dc}}) + U_{\mathrm{dc\_dc}} \tag{9}$$

where $\varphi_{u\mathrm{dc}}$ is the initial phase of the ac component.

Since the dc component is much larger than the amplitude of the ac component (i.e., $U_{\mathrm{dc\_dc}} >> U_{\mathrm{dc\_ac}}$), substituting (9) into (7), then (10) can be expressed as follows:

$$C \frac{\mathrm{d}U_{\mathrm{dc}}}{\mathrm{d}t} U_{\mathrm{dc}} \doteq C \cdot 2\omega_{\mathrm{f}} \cdot U_{\mathrm{dc\_ac}} \cdot U_{\mathrm{dc\_dc}} \cos(2\omega_{\mathrm{f}} t + \varphi_{u\mathrm{dc}}). \tag{10}$$

According to (7), (8), and (10), the amplitude of the ac component in the dc bus voltage can be calculated as follows:

$$U_{\mathrm{dc\_ac}} = \frac{1}{C \cdot 2\omega_{\mathrm{f}} \cdot U_{\mathrm{dc\_dc}}} \sqrt{Q_{\mathrm{c}}^{\mathrm{out}\,2} + Q_{\mathrm{s}}^{\mathrm{out}\,2}}. \tag{11}$$

To investigate the relationship between the NS active and reactive currents $i_{\mathrm{d}}^{\mathrm{n}}$ and $i_{\mathrm{q}}^{\mathrm{n}}$, (11) can be derived as follows:

$$\begin{aligned} &U_{\mathrm{dc\_ac}} \\ &= k_{\mathrm{dc}} \sqrt{a^2 + b^2} \sqrt{\left(i_{\mathrm{d}}^{\mathrm{n}} + \frac{ac_1 - bc_2}{a^2 + b^2}\right)^2 + \left(i_{\mathrm{q}}^{\mathrm{n}} + \frac{ac_2 + bc_1}{a^2 + b^2}\right)^2} \end{aligned} \tag{12}$$

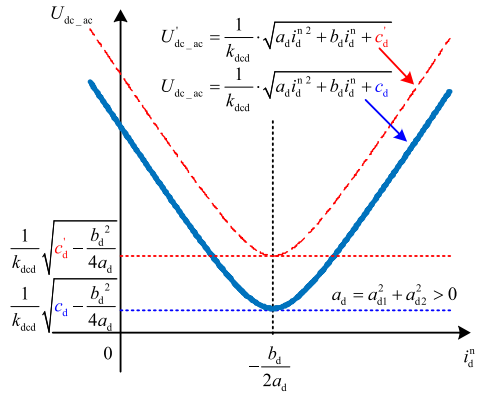

Fig. 2. Mechanism between the DC bus voltage ripple amplitude $U_{\mathrm{dc\_ac}}$ and the NS active current $i_{\mathrm{d}}^{\mathrm{n}}$.

where

$$\begin{cases} k_{\mathrm{dc}} = 3/(4\omega_{\mathrm{f}} \cdot U_{\mathrm{dc\_dc}} C) \\ a = v_{\mathrm{d}}^{\mathrm{p}} \\ b = v_{\mathrm{q}}^{\mathrm{p}} \\ c_1 = v_{\mathrm{d}}^{\mathrm{n}} i_{\mathrm{d}}^{\mathrm{p}} + v_{\mathrm{q}}^{\mathrm{n}} i_{\mathrm{q}}^{\mathrm{p}} \\ c_2 = v_{\mathrm{q}}^{\mathrm{n}} i_{\mathrm{d}}^{\mathrm{p}} - v_{\mathrm{d}}^{\mathrm{n}} i_{\mathrm{q}}^{\mathrm{p}}. \end{cases} \tag{13}$$

As can be seen from (12), when $i_{\mathrm{d}}^{\mathrm{n}}$ is $-\frac{ac_1 - bc_2}{a^2 + b^2}$ and $i_{\mathrm{q}}^{\mathrm{n}}$ is $-\frac{ac_2 + bc_1}{a^2 + b^2}$, the amplitude of the dc bus voltage ripple $U_{\mathrm{dc\_ac}}$ is zero. Meanwhile, when the reactive current $i_{\mathrm{q}}^{\mathrm{n}}$ changes, the active current $i_{\mathrm{d}}^{\mathrm{n}}$ that can minimize the dc bus voltage ripple will not change. Thus, the active and reactive currents have the similar relationship with the dc bus voltage ripple amplitude, and they are independent from each other.

Furthermore, in order to analyze the mechanism between the dc bus voltage ripple amplitude and the NS active current, the NS active current $i_{\mathrm{d}}^{\mathrm{n}}$ is selected as the independent variable, and the reactive current $i_{\mathrm{q}}^{\mathrm{n}}$ is fixed as a constant. Substituting (6) into (11), then (14) can be obtained as follows:

$$U_{\mathrm{dc\_ac}} = \frac{1}{k_{\mathrm{dcd}}} \cdot \sqrt{a_{\mathrm{d}} i_{\mathrm{d}}^{\mathrm{n}\,2} + b_{\mathrm{d}} i_{\mathrm{d}}^{\mathrm{n}} + c_{\mathrm{d}}} \tag{14}$$

where

$$\begin{cases} a_{\mathrm{d}} = v_{\mathrm{d}}^{\mathrm{p}\,2} + v_{\mathrm{q}}^{\mathrm{p}\,2} \\ b_{\mathrm{d}} = 2[v_{\mathrm{d}}^{\mathrm{p}}(v_{\mathrm{d}}^{\mathrm{n}} i_{\mathrm{d}}^{\mathrm{p}} + v_{\mathrm{q}}^{\mathrm{n}} i_{\mathrm{q}}^{\mathrm{p}}) - v_{\mathrm{q}}^{\mathrm{p}}(v_{\mathrm{q}}^{\mathrm{n}} i_{\mathrm{d}}^{\mathrm{p}} - v_{\mathrm{d}}^{\mathrm{n}} i_{\mathrm{q}}^{\mathrm{p}})] \\ c_{\mathrm{d}} = (v_{\mathrm{d}}^{\mathrm{n}} i_{\mathrm{d}}^{\mathrm{p}} + v_{\mathrm{q}}^{\mathrm{n}} i_{\mathrm{q}}^{\mathrm{p}} + v_{\mathrm{q}}^{\mathrm{p}} i_{\mathrm{q}}^{\mathrm{n}})^2 + (v_{\mathrm{q}}^{\mathrm{n}} i_{\mathrm{d}}^{\mathrm{p}} - v_{\mathrm{d}}^{\mathrm{n}} i_{\mathrm{q}}^{\mathrm{p}} + v_{\mathrm{d}}^{\mathrm{p}} i_{\mathrm{q}}^{\mathrm{n}})^2 \\ k_{\mathrm{dcd}} = (4\omega_{\mathrm{f}} \cdot U_{\mathrm{dc\_dc}} C)/3. \end{cases} \tag{15}$$

It can be seen from (14) that the amplitude of the dc bus voltage ripple and the NS active current have a parabolic-like relationship, as shown in Fig. 2. Since $a_{\mathrm{d}} = v_{\mathrm{d}}^{\mathrm{p}\,2} + v_{\mathrm{q}}^{\mathrm{p}\,2} > 0$, $U_{\mathrm{dc\_ac}}$ has the minimum value when $i_{\mathrm{d}}^{\mathrm{n}}$ varies. Specifically, when the NS active current $i_{\mathrm{d}}^{\mathrm{n}}$ is set as follows:

$$i_{\mathrm{d}}^{\mathrm{n}} = -\frac{b_{\mathrm{d}}}{2a_{\mathrm{d}}} = -\frac{v_{\mathrm{d}}^{\mathrm{p}} v_{\mathrm{d}}^{\mathrm{n}} i_{\mathrm{d}}^{\mathrm{p}} + v_{\mathrm{d}}^{\mathrm{p}} v_{\mathrm{q}}^{\mathrm{n}} i_{\mathrm{q}}^{\mathrm{p}} - v_{\mathrm{q}}^{\mathrm{p}} v_{\mathrm{q}}^{\mathrm{n}} i_{\mathrm{d}}^{\mathrm{p}} + v_{\mathrm{q}}^{\mathrm{p}} v_{\mathrm{d}}^{\mathrm{n}} i_{\mathrm{q}}^{\mathrm{p}}}{v_{\mathrm{d}}^{\mathrm{p}\,2} + v_{\mathrm{q}}^{\mathrm{p}\,2}}. \tag{16}$$

The amplitude of the dc bus voltage ripple obtains the minimum value, which can be written as follows:

$$U_{\text{dc\_ac min}} = \frac{1}{k_{\text{dcd}}}\sqrt{c_{\text{d}} - \frac{b_{\text{d}}^2}{4a_{\text{d}}}}. \tag{17}$$

It can be seen from (16) that the NS active current to minimize the voltage ripple is determined by the rectifier voltage v and the positive sequence currents i_{d}^{p}, and i_{q}^{p}. According to (15) and (17), when the reactive current i_{q}^{n} changes, the minimum of the voltage ripple will change. But the symmetry axis $-b_{\text{d}}/(2a_{\text{d}})$ will not change, as shown in Fig. 2. Thus, the active current i_{d}^{n} is not correlated with the reactive current i_{q}^{n}. In addition, it is also independent of the dc bus capacitance C, as well as the grid angular frequency ω_{f}. Therefore, by shaping the NS active current and observing the corresponding amplitude of the dc bus voltage ripple, the curve between them can be fitted by the data-driven method. Then, the NS active current $i_{\text{d}}^{\text{n}} = -b_{\text{d}}/(2a_{\text{d}})$ can be calculated, so as to suppress the dc bus voltage ripple effectively in theory.

Similarly, when the active current i_{d}^{n} is fixed as a constant, and the reactive current i_{q}^{n} is selected as the independent variable, the dc bus voltage ripple amplitude can be also calculated as follows:

$$U_{\text{dc\_ac}} = \frac{1}{k_{\text{dcd}}} \cdot \sqrt{a_{\text{q}} {i_{\text{q}}^{\text{n}}}^2 + b_{\text{q}} i_{\text{q}}^{\text{n}} + c_{\text{q}}} \tag{18}$$

where

$$\begin{cases} a_{\text{q}} = {v_{\text{d}}^{\text{p}}}^2 + {v_{\text{q}}^{\text{p}}}^2 \\ b_{\text{q}} = 2[v_{\text{q}}^{\text{p}}(v_{\text{d}}^{\text{n}} i_{\text{d}}^{\text{p}} + v_{\text{q}}^{\text{n}} i_{\text{q}}^{\text{p}}) + v_{\text{d}}^{\text{p}}(v_{\text{q}}^{\text{n}} i_{\text{d}}^{\text{p}} - v_{\text{d}}^{\text{n}} i_{\text{q}}^{\text{p}})] \\ c_{\text{q}} = (v_{\text{d}}^{\text{n}} i_{\text{d}}^{\text{p}} + v_{\text{q}}^{\text{n}} i_{\text{q}}^{\text{p}} + v_{\text{d}}^{\text{p}} i_{\text{d}}^{\text{n}})^2 + (v_{\text{q}}^{\text{n}} i_{\text{d}}^{\text{p}} - v_{\text{d}}^{\text{n}} i_{\text{q}}^{\text{p}} - v_{\text{q}}^{\text{p}} i_{\text{d}}^{\text{n}})^2. \end{cases} \tag{19}$$

And the reactive current i_{q}^{n}, which can minimize the dc bus voltage ripple can be addressed as follows:

$$i_{\text{q}}^{\text{n}} = -\frac{b_{\text{q}}}{2a_{\text{q}}} = -\frac{v_{\text{q}}^{\text{p}} v_{\text{d}}^{\text{n}} i_{\text{d}}^{\text{p}} + v_{\text{q}}^{\text{p}} v_{\text{q}}^{\text{n}} i_{\text{q}}^{\text{p}} + v_{\text{d}}^{\text{p}} v_{\text{q}}^{\text{n}} i_{\text{d}}^{\text{p}} - v_{\text{d}}^{\text{p}} v_{\text{d}}^{\text{n}} i_{\text{q}}^{\text{p}}}{{v_{\text{d}}^{\text{p}}}^2 + {v_{\text{q}}^{\text{p}}}^2}. \tag{20}$$

Thus, by sequentially changing the NS currents, and calculating the reference currents, the purpose of the dc bus voltage ripple suppression can be achieved.

B. Implementation of the Proposed Method

The control block diagram of the data-driven adaptive NS current control method is shown in Fig. 3. As one can see, the positive sequence active reference current $i_{\text{d}}^{\text{p}*}$ is generated by the voltage loop, and the positive sequence reactive reference current $i_{\text{q}}^{\text{p}*}$ is set as zero to improve the power factor. Meanwhile, the NS reference currents are generated by the proposed data-driven adaptive NS current controller. The final current reference can be calculated as follows:

$$\begin{cases} i_{\alpha}^{*} = i_{\alpha}^{\text{p}*} + i_{\alpha}^{\text{n}*} \\ i_{\beta}^{*} = i_{\beta}^{\text{p}*} + i_{\beta}^{\text{n}*} \end{cases}. \tag{21}$$

The data-driven adaptive NS current controller consists of three components: a band-pass filter (BPF), an online calculator for the dc bus voltage ripple amplitude, and an adaptive NS current generator. Among them, the BPF is employed to extract the ac component of the dc bus voltage. The transfer function of the BPF can be written as

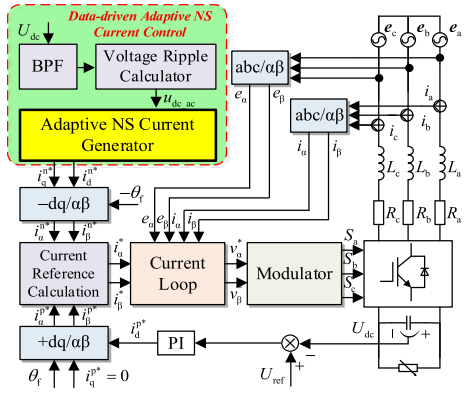

Fig. 3. Control block diagram of the data-driven adaptive current control method.

$$G_{\text{BPF}}(s) = \frac{(\omega_{\text{n}}/Q)s}{s^2 + (\omega_{\text{n}}/Q)s + \omega_{\text{n}}^2} \tag{22}$$

where $\omega_{\text{n}} = 2\,\omega_{\text{f}}$ is the center frequency of the BPF and Q is the quality factor, which determines the respective bandwidth and tracking speed of the BPF. In order to select a proper quality factor Q, the relationship between Q and tracking speed should be established. The transfer function of a sinusoidal input signal is obtained as follows:

$$E(s) = L[e(t)] = L[\sin(\omega_{\text{n}} t)] = \frac{\omega_{\text{n}}}{s^2 + \omega_{\text{n}}^2}. \tag{23}$$

According to (22) and (23), the transfer function of the output signal can be written as follows:

$$R(s) = E(s)G_{\text{BPF}}(s) = \frac{\omega_{\text{n}}}{s^2 + \omega_{\text{n}}^2} - \frac{\omega_{\text{n}}}{s^2 + \omega_{\text{n}}/Qs + \omega_{\text{n}}^2}. \tag{24}$$

The time domain expression of the output signal is further derived as follows:

$$r(t) = L^{-1}[R(s)] =$$

$$\begin{cases} \sin(\omega_{\text{n}} t) + \frac{1}{2\sqrt{\frac{1}{4Q^2} - 1}} e^{-\frac{\omega_{\text{n}}}{2Q} t}\left[e^{-\sqrt{\frac{1}{4Q^2} - 1}\omega_{\text{n}} t} - e^{\sqrt{\frac{1}{4Q^2} - 1}\omega_{\text{n}} t}\right] & 0.5 > Q > 0 \\ \sin(\omega_{\text{n}} t) - e^{-\frac{\omega_{\text{n}}}{2Q} t}\omega_{\text{n}} t & Q = 0.5 \\ \sin(\omega_{\text{n}} t) - \frac{1}{\sqrt{1 - \frac{1}{4Q^2}}} e^{-\frac{\omega_{\text{n}}}{2Q} t} \sin\left(\sqrt{1 - \frac{1}{4Q^2}}\omega_{\text{n}} t\right) & Q > 0.5 \end{cases} \tag{25}$$

where $\sin(\omega_{\text{n}} t)$ is the input signal, the tracking error $\text{error}(t)$ can be expressed as follows:

$$\text{error}(t) = e(t) - r(t) =$$

$$\begin{cases} -\frac{1}{2\sqrt{\frac{1}{4Q^2} - 1}} e^{-\frac{\omega_{\text{n}}}{2Q} t}\left[e^{-\sqrt{\frac{1}{4Q^2} - 1}\omega_{\text{n}} t} - e^{\sqrt{\frac{1}{4Q^2} - 1}\omega_{\text{n}} t}\right] & 0.5 > Q > 0 \\ e^{-\frac{\omega_{\text{n}}}{2Q} t}\omega_{\text{n}} t & Q = 0.5 \\ \frac{1}{\sqrt{1 - \frac{1}{4Q^2}}} e^{-\frac{\omega_{\text{n}}}{2Q} t} \sin\left(\sqrt{1 - \frac{1}{4Q^2}}\omega_{\text{n}} t\right) & Q > 0.5 \end{cases}. \tag{26}$$

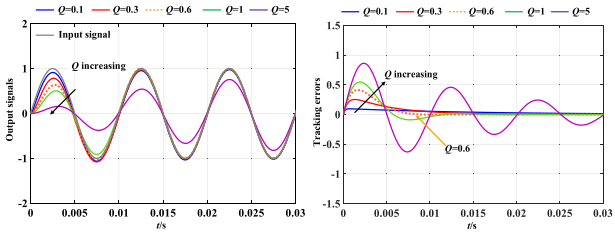

(a) (b)

Fig. 4. Signal waveforms of the BPF with different quality factor Q. (a) Input and output signals. (b) Tracking error signals.

According to (26), the faster error(t) decreases to near 0, the faster the BPF can track the input signal. The signal waveforms of the BPF with varying Q are plotted in Fig. 4. As one can see from Fig. 4(a), with the quality factor Q increases, the tracking speed will be slower. It can be also seen from Fig. 4(b) that when $Q < 0.5$, the error signal is a continuously decreasing dc signal, degrading the accuracy of the magnitude calculation. When $Q > 1$, there is oscillation in the tracking error. Therefore, to ensure the tracking speed and bandwidth, Q should be in the range between 0.5 and 1. In this article, $Q = 0.6$ is chosen as a compromise and as a result, the BPF can track the input signal within 10 ms.

Then, the online calculation of the dc bus voltage second-order ripple amplitude is given in

$$U_{\mathrm{dc\_ac}} = \sqrt{\frac{\sum_{i=1}^{N}\left[u_{\mathrm{dc\_ac}}(i)\right]^2}{N}} \tag{27}$$

where $N = T_{\mathrm{f}}/T_{\mathrm{s}}$ is the total number of the samples in each grid cycle T_{f}, and $u_{\mathrm{dc\_ac}}(i)$ is the ith output value of the BPF.

The flow chart of the data-driven adaptive NS current generator is, as shown in Fig. 5. The process has four main stages as follows.

1) Activating judgment: When the dc bus voltage ripple amplitude $U_{\mathrm{dc\_ac}}$ and duration t_{ton} are greater than the set values U_{set} and t_{set}, respectively, the NS current controller is activated to suppress the dc bus voltage. The setting value can be adjusted according to the actual conditions to meet different requirements. The smaller the U_{set} and t_{set}, the more sensitive the activating-judgment is, and the higher the power quality can be met. Conversely, the fault-tolerant operation can also be satisfied.

2) Initial current reference estimation: The initial value of the NS current needs to be determined. On the one hand, if the NS current is too large, it is harmful for the power quality of the system. On the other hand, if the NS current is too small, the change of the dc bus voltage ripple amplitude is difficult to be observed, which brings a negative impact on the reference current solution. Thus, the principle of selecting the initial NS current is obtained as follows: Under the condition that the dc bus voltage ripple changing can be observed, the NS current should be as small as possible. Therefore, the initial NS current amplitudes can be given, according to a proportion of the positive sequence active current, which are $i^{\mathrm{n}}_{\mathrm{dref0}} = \lambda_{\mathrm{d}} i^{\mathrm{p}*}_{\mathrm{d}}$, and

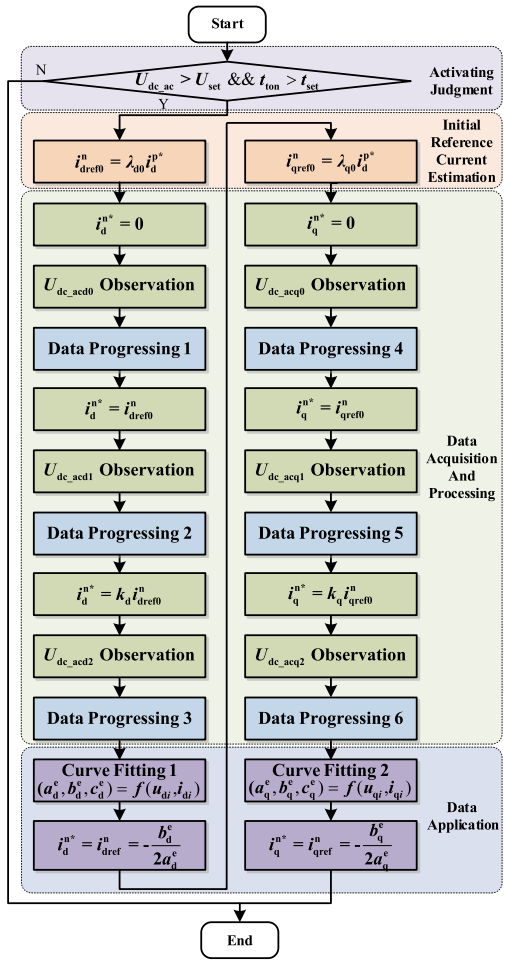

Fig. 5. Flow chart of the data-driven adaptive NS current generator.

$i^{\mathrm{n}}_{\mathrm{qref0}} = \lambda_{\mathrm{q}} i^{\mathrm{p}*}_{\mathrm{d}}$. In addition, λ_{d} and λ_{q} are the NS current factors, which can be flexibly adjusted according to different operating conditions. Generally, when λ_{d} and λ_{q} are about in the range of [0.1, 0.2], the above-mentioned principle can be satisfied. In this article, the NS current factors are defined as follows, $\lambda_{\mathrm{d}} = 0.15$ and $\lambda_{\mathrm{q}} = 0.1$.

3) Data acquisition: The corresponding dc bus voltage ripple amplitude data is observed, according to the NS current. As can be seen from Fig. 2 and (14), to solve the relationship between the NS active current and the dc bus voltage ripple amplitude through the data, three parameters (i.e., a_{d}, b_{d}, and c_{d}) need to be determined. Thus, at least three types of data need to be captured. In other words, three different NS currents and the corresponding voltage ripple amplitudes need to be observed. Assuming that the grid current can track the reference current in the steady state, that is

$$\begin{cases} i^{\mathrm{n}*}_{\mathrm{d}} = i^{\mathrm{n}}_{\mathrm{d}} \\ i^{\mathrm{n}*}_{\mathrm{q}} = i^{\mathrm{n}}_{\mathrm{q}}. \end{cases} \tag{28}$$

Hence, the NS current can be controlled by adjusting the current reference. Thus, the NS reference currents are set to 0, $i^{\mathrm{n}}_{\mathrm{ref0}}$, and $k\, i^{\mathrm{n}}_{\mathrm{ref0}}$ in turn, where $k \in (0, 1)$ is the coefficient to

determine the distance between the NS currents. Commonly, k can be set to 0.5 to keep the distance between the NS currents. Then, the corresponding second-order ripple amplitude of the dc bus voltage is observed. As a result, the required data can be obtained.

4) Data application: The obtained data are applied to fit the curve of the dc bus voltage ripple amplitude versus the NS current, where u_i and i_i represent the ith online observational data of the dc bus voltage ripple amplitude and the NS reference current, respectively. Then, the NS reference current that minimizes the dc bus voltage ripple can be calculated.

Since the process of fitting the curves is the same, the NS active current is employed as an example to give a specific illustration in this article.

C. Data-Driven Reference Current Calculation

As can be seen from (14) and (18), the mechanisms between the dc bus voltage ripple amplitude and the active or reactive currents are similar. Therefore, this section takes the active current as an example to give the calculation method of the reference current.

Equation (14) can be further derived as follows:

$$(k_{\mathrm{dcd}}U_{\mathrm{dc\_ac}})^2 = a_{\mathrm{d}}{i_{\mathrm{d}}^{\mathrm{n}}}^2 + b_{\mathrm{d}}i_{\mathrm{d}}^{\mathrm{n}} + c_{\mathrm{d}}. \tag{29}$$

Assuming that the ith observations of the dc bus voltage ripple amplitude and the NS active reference current are $u_{\mathrm{d}i}$ and $i_{\mathrm{d}i}$, respectively, and the total number of the observations is n, the sum of the squared observation errors can be expressed as follows:

$$L(a_{\mathrm{d}}, b_{\mathrm{d}}, c_{\mathrm{d}}) = \sum_{i=1}^{n}\left[(k_{\mathrm{dcd}}u_{\mathrm{d}i})^2 - (a_{\mathrm{d}}i_{\mathrm{d}i}^2 + b_{\mathrm{d}}i_{\mathrm{d}i} + c_{\mathrm{d}})\right]^2. \tag{30}$$

The cost function $L(a_{\mathrm{d}}, b_{\mathrm{d}}, c_{\mathrm{d}}) \geq 0$ is minimized when the partial derivatives of a_{d}, b_{d}, and c_{d} are 0, respectively. Thus, (31) can be noted as follows:

$$\begin{cases} \frac{\partial L}{\partial a_{\mathrm{d}}} = 2\sum_{i=1}^{n}\left[(k_{\mathrm{dcd}}u_{\mathrm{d}i})^2 - (a_{\mathrm{d}}i_{\mathrm{d}i}^2 + b_{\mathrm{d}}i_{\mathrm{d}i} + c_{\mathrm{d}})\right]i_{\mathrm{d}i}^2 = 0 \\ \frac{\partial L}{\partial b_{\mathrm{d}}} = 2\sum_{i=1}^{n}\left[(k_{\mathrm{dcd}}u_{\mathrm{d}i})^2 - (a_{\mathrm{d}}i_{\mathrm{d}i}^2 + b_{\mathrm{d}}i_{\mathrm{d}i} + c_{\mathrm{d}})\right]i_{\mathrm{d}i} = 0 \\ \frac{\partial L}{\partial c_{\mathrm{d}}} = 2\sum_{i=1}^{n}\left[(k_{\mathrm{dcd}}u_{\mathrm{d}i})^2 - (a_{\mathrm{d}}i_{\mathrm{d}i}^2 + b_{\mathrm{d}}i_{\mathrm{d}i} + c_{\mathrm{d}})\right] = 0. \end{cases} \tag{31}$$

Then, to estimate a_{d}, b_{d}, and c_{d} based on the sample data, $a_{\mathrm{d}}^{\mathrm{e}}$, $b_{\mathrm{d}}^{\mathrm{e}}$, $c_{\mathrm{d}}^{\mathrm{e}}$ can be calculated as follows:

$$\begin{bmatrix} a_{\mathrm{d}}^{\mathrm{e}} \\ b_{\mathrm{d}}^{\mathrm{e}} \\ c_{\mathrm{d}}^{\mathrm{e}} \end{bmatrix} = \begin{bmatrix} \sum_{i=1}^{n}(i_{\mathrm{d}i}^4) & \sum_{i=1}^{n}(i_{\mathrm{d}i}^3) & \sum_{i=1}^{n}(i_{\mathrm{d}i}^2) \\ \sum_{i=1}^{n}(i_{\mathrm{d}i}^3) & \sum_{i=1}^{n}(i_{\mathrm{d}i}^2) & \sum_{i=1}^{n}(i_{\mathrm{d}i}^1) \\ \sum_{i=1}^{n}(i_{\mathrm{d}i}^2) & \sum_{i=1}^{n}(i_{\mathrm{d}i}^1) & \sum_{i=1}^{n}(i_{\mathrm{d}i}^0) \end{bmatrix}^{-1} \times \begin{bmatrix} \sum_{i=1}^{n}(k_{\mathrm{dcd}}u_{\mathrm{d}i})^2 i_{\mathrm{d}i}^2 \\ \sum_{i=1}^{n}(k_{\mathrm{dcd}}u_{\mathrm{d}i})^2 i_{\mathrm{d}i} \\ \sum_{i=1}^{n}(k_{\mathrm{dcd}}u_{\mathrm{d}i})^2 \end{bmatrix}. \tag{32}$$

Furthermore, the NS active reference current can be derived as follows:

$$i_{\mathrm{dref}}^{\mathrm{n}} = -\frac{b_{\mathrm{d}}^{\mathrm{e}}}{2a_{\mathrm{d}}^{\mathrm{e}}}. \tag{33}$$

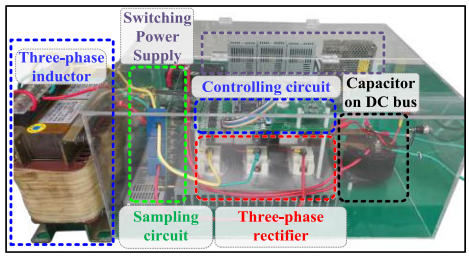

Fig. 6. Experimental platform.

Similarly, the NS reactive reference current can be addressed as follows:

$$i_{\mathrm{qref}}^{\mathrm{n}} = -\frac{b_{\mathrm{q}}^{\mathrm{e}}}{2a_{\mathrm{q}}^{\mathrm{e}}}. \tag{34}$$

Finally, by employing $i_{\mathrm{dref}}^{\mathrm{n}}$, and $i_{\mathrm{qref}}^{\mathrm{n}}$ as the NS reference currents, the purpose of the dc bus voltage second-order ripple suppression can be achieved.

D. Comparison With the State-of-the-Art

A comparison of the proposed method with the state-of-the-art is shown in Table I. Compared with the improved proportional quasi resonant (IPQR) controller in [17], the proposed method can achieve synergistic suppression of the dc bus voltage ripple and the grid harmonic currents. Compared with the output power control (OPC) method in [19], this method does not require the positive and NS decompositions, which reduces the system complexity. Compared with the DPC methods in [23] and [24], this method has a strong robustness against the grid inductance variation. This is because the inductance is not required in the reference current calculation. Compared with the voltage sensorless model predictive power control (MPPC) method in [25], this method upgrades the mode of reference current calculation from the model-driven to the data-driven. Since the grid and rectifier voltages are not required in the reference current calculation, it can effectively avoid the performance degradation. As a short summary here, this method provides a feasible and reliable option for the dc bus voltage ripple suppression.

IV. Experimental Verification

To verify the effectiveness of the proposed method, a 3 kW experimental prototype is built. Table II gives the experimental parameters. GJAC-PSA 33010 is used as the programmable three-phase ac power source and ITECH 8904E is employed as the electronic load. The experimental platform is shown in Fig. 6.

A. Complicated Unbalanced Grid Conditions

In order to verify the control performance of the proposed method, experimental results and analysis under complicated unbalanced grid conditions are given in this section. Considering the complicated unbalanced grid condition that the grid frequency is shifted to 52 Hz, the three-phase voltage rms values are 50 V, 110 V, and 80 V, respectively, and the phases are

TABLE I
COMPARISON WITH THE STATE-OF-THE-ART

Category		IPQR in [17]	OPC in [19]	DPC in [23]	DPC with inductance identification in [24]	Voltage-sensorless MPPC in [25]	Proposed method
Inductance robustness (Yes is better)		**Yes**	No	No	**Yes**	No	**Yes**
DC bus voltage ripple suppression (Yes is better)		No	**Yes**	**Yes**	**Yes**	**Yes**	**Yes**
Output power model (No is better)		**No**	Yes	Yes	Yes	Yes	**No**
Sequence extraction (No is better)		**No**	Yes	**No**	**No**	**No**	**No**
Parameters in reference current calculation (No is better)	e	**No**	Yes	Yes	Yes	**No**	**No**
	v	**No**	Yes	Yes	Yes	Yes	**No**

TABLE II
EXPERIMENTAL PARAMETERS

Parameters/Unit	Values
Three-phase grid voltages (RMS): e/V	50/110/80(110)
Phases of the grid voltages:φ_e/°	0/230(240)/130(120)
Fundamental frequency: f_f/Hz	52/50
DC bus capacitance C: μF	200
DC bus voltage: U_{dc}/V	300
Output power: P_{Load}/kW	3
Load resistance: R_L/Ω	30
Switching frequency: f/kHz	5
Sampling time: T_s/ms	0.2

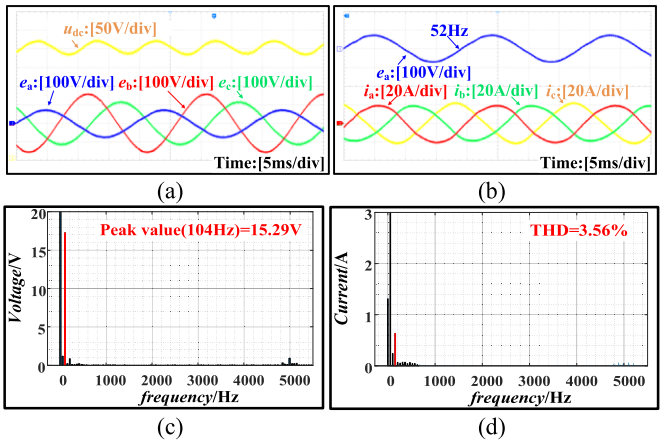

Fig. 7. Experimental waveforms under complicated unbalanced grid. (a) DC bus voltage and three-phase grid voltages. (b) Grid voltage of Phase-a, and three-phase grid currents. (c) Fourier analysis of the dc bus voltage. (d) Fourier analysis of the Phase-a grid current.

0°, 230°, and 130°, respectively. Fig. 7 provides the experimental waveforms of the rectifier before the dc bus, voltage ripple suppression. As can be seen from Fig. 7, the dc bus voltage ripple amplitude is 15.29 V, and the grid current rms values are 14.6 A, 13.4 A, and 14.7 A, respectively. Besides, the amplitudes of the third-order harmonic current are 0.63 A, 0.69 A, 0.72 A, respectively, and the total harmonic distortions (THDs) are 3.6%, 4.1%, and 4.0%, respectively. As a result, there is an obvious voltage ripple in the dc bus. Meanwhile, the three-phase currents

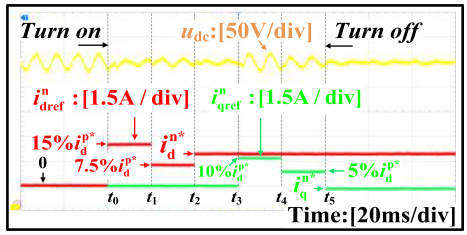

Fig. 8. Experimental waveform of the dynamic response to suppress DC bus voltage ripple.

are severely distorted and contain the third-order harmonic current.

To illustrate the procedure of the proposed method, Fig. 8 shows the experimental waveform of the dynamic response to suppress dc bus voltage ripple. Before t_0, the NS active and reactive reference currents (i_d^{n*} and i_q^{n*}) are 0, and the voltage ripple amplitude of the dc bus is 15.29 V. From t_0 to t_2, the NS active reference current i_d^{n*} is set to 15% and 7.5% of i_d^{p*}, respectively. To be specific, i_d^{n*} is 2.4 A and 1.2 A, respectively. According to (14), when the NS active current is shaped, the voltage ripple amplitude of the dc bus will change correspondingly. As one can see, the voltage ripple amplitude is 7.17 V and 5.71 V, respectively. Based on the above-mentioned data and (32), a_d^e is 48260 and b_d^e is -163800, respectively. Thus, the final NS active reference current $i_{dref}^n = -b_d^e/(2a_d^e)$ is 1.69 A. During the interval between t_2 and t_3, the dc bus voltage ripple is 3.62 V while the NS reactive current is 0. From t_3 to t_5, the NS reactive current is shaped to 1.6 A and 0.8 A, respectively. And the dc bus voltage ripple is 15.10 V and 8.75 V, respectively. Similarly, based on the experimental data, it can be calculated that a_q^e is 43380 and b_q^e is 15350, respectively. Therefore, the final reactive reference current $i_{qref}^n = -b_q^e/(2a_q^e)$ is -0.18 A. At t_5, the reactive reference current i_q^{n*} is set to i_{qref}^n. Subsequently, the dc bus voltage ripple disappears. Thus, the experiment results verify the feasibility of the adaptive NS current generator, as shown in Fig. 5. Meanwhile, the effectiveness of the data-driven reference current calculation in Section III-C can be also demonstrated.

The experimental waveforms with the proposed method are given in Fig. 9. As one can see, the voltage ripple amplitude

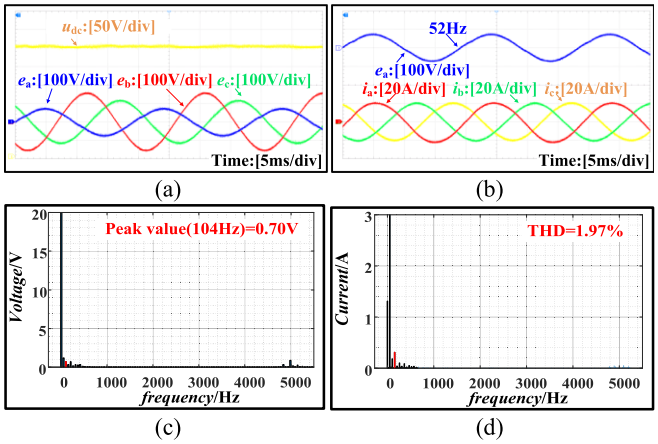

Fig. 9. Experimental waveforms with the proposed method. (a) DC bus voltage and three-phase grid voltages. (b) Grid voltage of Phase-a, and three-phase grid currents. (c) Fourier analysis of the DC bus voltage. (d) Fourier analysis of the Phase-a grid current.

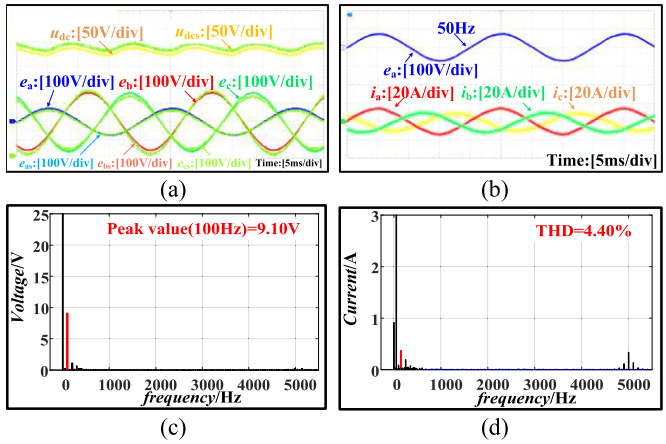

Fig. 10. Experimental waveforms with existing DPC [23]. (a) DC bus voltage and three-phase grid voltages. (b) Grid voltage of Phase-a, and three-phase grid currents. (c) Fourier analysis of the DC bus voltage. (d) Fourier analysis of the Phase-a grid current.

of the dc bus is only 0.7 V, which is only 0.23% of the dc bus voltage component (300 V). Therefore, the reference current calculated by the proposed method can effectively suppress the dc bus voltage ripple. At the same time, the rms values of the grid currents are 15.13 A, 14.23 A, and 14.25 A, respectively, while the third-order harmonic currents are 0.31 A, 0.16 A, and 0.19 A, respectively. In addition, the THDs are reduced to 1.97%, 1.81%, and 1.69%, respectively. Thus, after the suppression of the dc bus voltage ripple, the odd harmonics of the grid current can be indirectly reduced. As a result, the proposed method can achieve good performance under the complicated unbalanced grid.

B. Voltage Sampling Errors Conditions

To further verify the robustness of the proposed method, the experimental results and analysis under the voltage sampling error condition are presented in this section.

As a comparison, the experimental waveforms of the existing DPC and the proposed method are given in Figs. 10 and 11, respectively. And the quantitative comparison of the two methods is shown in Fig. 12. Where e_{as}, e_{bs}, e_{cs}, and u_{dcs} are the sampling values of the three-phase and dc bus voltages, respectively. As can be seen from Fig. 10, the rms values of the three-phase voltages are 50 V, 110 V, and 110 V, respectively. Meanwhile, the sampling values are 0.9, 1.1, and 0.9 times of the actual values, respectively. L' is 0.8L, where L' is the inductance employed to calculate the reference power in DPC. In addition, the sampling value of the dc bus voltage u_{dcs} is 300 V (1.05 times of the actual voltage). The dc bus voltage sampling error is smaller than that of the grid voltages, for the dc bus voltage sampling error will directly change the output voltage. As one can see, due to the voltage close-loop control, the actual voltage of the dc bus is only 286 V. And the excessive error may cause the rectifier cannot work in the PWM rectification. However, since the DPC [23] relies on the grid voltage sampling and the inductance L'

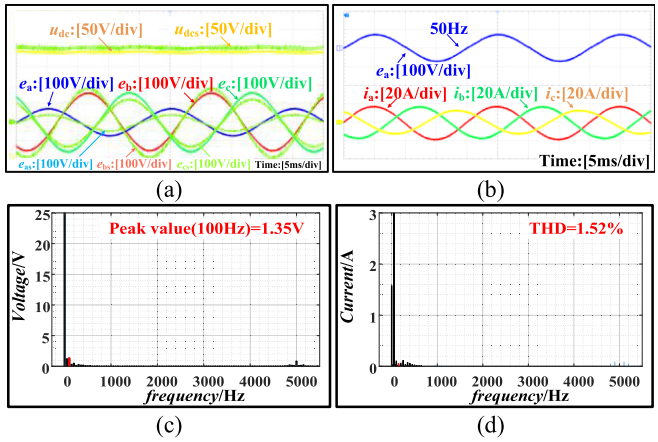

Fig. 11. Experimental waveforms with the proposed method. (a) DC bus voltage and Three-phase grid voltages. (b) Grid voltage of Phase-a, and three-phase grid currents. (c) Fourier analysis of the DC bus voltage. (d) Fourier analysis of the Phase-a grid current.

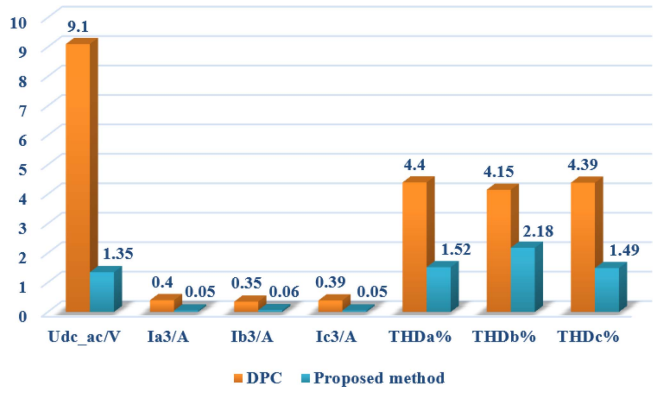

Fig. 12. Quantitative comparison of the proposed method with DPC.

to calculate the compensating power, there are errors in the final reference power, which cannot effectively suppress the dc bus voltage ripple. As can be seen from Fig. 10(c), the voltage ripple amplitude is 9.10 V, which is 3.0% of the dc component of the bus voltage. Correspondingly, the third-order harmonic of the grid current cannot be completely reduced. Furthermore, the amplitudes of the third-order harmonic currents I_{a3}, I_{b3}, and I_{c3} are 0.40 A, 0.35 A, and 0.39 A, respectively, and the THDs are 4.40%, 4.12%, and 4.35%, respectively. Thus, the existing DPC cannot achieve the good performance under the voltage sampling and inductance errors condition.

The experimental waveforms of the proposed control method under the same unbalanced condition are given in Fig. 11. As one can see, the three-phase voltage sampling values are 0.6, 1.2, and 0.8 times of the actual values, respectively. Thus, the sampling error is larger than that of the existing method. And the dc bus voltage sampling value is 1.05 times of the actual value. For the proposed method do not need the inductance L' to calculate the reference current, the inductance error can be ignored. As can be seen from Fig. 11, under the more severe sampling error condition, the dc bus voltage ripple amplitude is only 1.35 V, which is just 0.47% of the dc bus voltage component. Meanwhile, the amplitudes of the third-order harmonic currents I_{a3}, I_{b3}, and I_{c3} are 0.05 A, 0.06 A, and 0.05 A, respectively, and the THDs are 1.52%, 2.18%, and 1.49%, respectively. Thus, the harmonic currents can also be effectively reduced. As can be seen from Fig. 12, the dc bus voltage ripple amplitude and the THDs of the proposed method is smaller than that of the DPC, which has a better performance. The main reasons are summarized as follows: On the one hand, the proposed method does not need the grid voltage to calculate the reference current, relieving the side effect of the sampling error; on the other hand, as can be seen from Fig. 2, when the dc bus voltage sampling error is linear, the curves will shift up or down, but it does not affect the symmetry axis of the curve. Hence, the proposed method shows strong robustness against the voltage sampling error.

V. Conclusion

In this article, the parabolic-like relationship between the dc bus voltage ripple amplitude and the NS current is revealed. When the NS currents are controlled as the symmetry axis of the parabolic-like curve, the dc bus voltage ripple will be minimized. Experimental results confirms that even under complicated unbalanced and voltage sampling error conditions, the proposed method still can effectively improve the power quality of the rectifier. Besides, the reference current calculation is upgraded from the model-driven to data-driven, which have a good robustness and resistance against the parameter drift. However, a certain time is required for data acquisition, which is limited by the required data types. The proposed method can show the performance of faster ripple suppression if reducing the requirement of the data types. Overall, this article provides an effective scheme for the cooperative suppression of the dc bus voltage ripple and the grid current harmonics under unbalanced grid conditions for EV charging system.

References

[1] G. Li, J. Ruan, K. Wang, Y. Deng, X. He, and Y. Wang, "An interleaved three-phase PWM single-stage resonant rectifier with high-frequency isolation," *IEEE Trans. Ind. Electron.*, vol. 67, no. 8, pp. 6572–6582, Aug. 2020.

[2] F. Wu, J. Zhao, Y. Liu, D. Zhou, and H. Luo, "Primary source inductive energy analysis based real-time multiple open-circuit fault diagnosis in two-level three-phase PWM boost rectifier," *IEEE Trans. Power Electron.*, vol. 33, no. 4, pp. 3411–3423, Apr. 2018.

[3] S. Lakhimsetty and V. T. Somasekhar, "A four-level open-end winding induction motor drive with a nested rectifier–inverter combination with two dc power supplies," *IEEE Trans. Power Electron.*, vol. 34, no. 9, pp. 8894–8904, Sep. 2019.

[4] W. Wu et al., "A virtual phase-lead impedance stability control strategy for the maritime VSC–HVDC system," *IEEE Trans. Ind. Inform.*, vol. 14, no. 12, pp. 5475–5486, Dec. 2018.

[5] X. Zhao, C. Chen, and J. Lai, "A high-efficiency active-boost-rectifier-based converter with a novel double-pulse duty cycle modulation for pv to DC microgrid applications," *IEEE Trans. Power Electron.*, vol. 34, no. 8, pp. 7462–7473, Aug. 2019.

[6] L. Xu et al., "A review of DC shipboard microgrids—Part II: Control architectures, stability analysis, and protection schemes," *IEEE Trans. Power Electron.*, vol. 37, no. 4, pp. 4105–4120, Apr. 2022.

[7] Y. Zhang, J. Fang, F. Gao, T. Song, S. Gao, and D. J. Rogers, "Second-harmonic ripple voltage suppression of integrated single-phase PWM rectifier charging system for EVs," *IEEE Trans. Power Electron.*, vol. 35, no. 4, pp. 3616–3626, Apr. 2020.

[8] Y. Zhang, J. Shan, Z. Huang, T. Song, and X. Zhu, "A dynamic equivalent current feedforward control strategy with variable reference current in three-phase PWM rectifiers," *IEEE Trans. Power Electron.*, vol. 39, no. 1, pp. 1636–1643, Jan. 2024.

[9] P. Wang, Y. Bi, F. Gao, T. Song, and Y. Zhang, "An improved dead-beat control method for single-phase PWM rectifiers in charging system for EVs," *IEEE Trans. Veh. Technol.*, vol. 68, no. 10, pp. 9672–9681, Oct. 2019.

[10] Y. Bi et al., "An improved combined current control for single-phase operation mode of single-/three-phase EV charging system with voltage ripple suppression," *IEEE Trans. Power Electron.*, vol. 38, no. 11, pp. 13635–13649, Nov. 2023.

[11] H. Zhao, Y. Shen, W. Ying, S. S. Ghosh, M. R. Ahmed, and T. Long, "A single- and three-phase grid compatible converter for electric vehicle on-board chargers," *IEEE Trans. Power Electron.*, vol. 35, no. 7, pp. 7545–7562, Jul. 2020.

[12] S.-Y. Cho, I.-O. Lee, J.-I. Baek, and G.-W. Moon, "Battery impedance analysis considering DC component in sinusoidal ripple-current charging," *IEEE Trans. Ind. Electron.*, vol. 63, no. 3, pp. 1561–1573, Mar. 2016.

[13] W. Jiang, Y. Wang, J. Wang, L. Wang, and H. Huang, "Maximizing instantaneous active power capability for PWM rectifier under unbalanced grid voltage dips considering the limitation of phase current," *IEEE Trans. Ind. Electron.*, vol. 63, no. 10, pp. 5998–6009, Oct. 2016.

[14] T. Song, Y. Zhang, F. Gao, X. Zhu, J. Shan, and Z. Kong, "Power model free voltage ripple suppression method of three-phase PWM rectifier under unbalanced grid," *IEEE Trans. Power Electron.*, vol. 37, no. 11, pp. 13799–13807, Nov. 2022.

[15] P. Rioual, H. Pouliquen, and J.-P. Louis, "Regulation of a PWM rectifier in the unbalanced network state using a generalized model," *IEEE Trans. Power Electron.*, vol. 11, no. 3, pp. 495–502, May 1996.

[16] M. Baumann and J. W. Kolar, "A novel control concept for reliable operation of a three-phase three-switch buck-type unity-power-factor rectifier with integrated boost output stage under heavily unbalanced mains condition," *IEEE Trans. Ind. Electron.*, vol. 52, no. 2, pp. 399–409, Apr. 2005.

[17] T. Song, P. Wang, Y. Zhang, F. Gao, Y. Tang, and S. Pholboon, "Suppression method of current harmonic for three-phase PWM rectifier in EV charging system," *IEEE Trans. Veh. Technol.*, vol. 69, no. 9, pp. 9634–9642, Sep. 2020.

[18] X. Guo, W. Liu, X. Zhang, X. Sun, Z. Lu, and J. M. Guerrero, "Flexible control strategy for grid-connected inverter under unbalanced grid faults without PLL," *IEEE Trans. Power Electron.*, vol. 30, no. 4, pp. 1773–1778, Apr. 2015.

[19] B. Yin, R. Oruganti, S. K. Panda, and A. K. S. Bhat, "An output-power-control strategy for a three-phase PWM rectifier under unbalanced supply conditions," *IEEE Trans. Ind. Electron.*, vol. 55, no. 5, pp. 2140–2151, May 2008.

[20] Z. Li, Y. Li, P. Wang, H. Zhu, C. Liu, and W. Xu, "Control of three-phase boost-type PWM rectifier in stationary frame under unbalanced input voltage," *IEEE Trans. Power Electron.*, vol. 25, no. 10, pp. 2521–2530, Oct. 2010.
[21] Y. Zhang and C. Qu, "Direct power control of a pulse width modulation rectifier using space vector modulation under unbalanced grid voltages," *IEEE Trans. Power Electron.*, vol. 30, no. 10, pp. 5892–5901, Oct. 2015.
[22] Y. Zhang, C. Qu, and J. Gao, "Performance improvement of direct power control of PWM rectifier under unbalanced network," *IEEE Trans. Power Electron.*, vol. 32, no. 3, pp. 2319–2328, Mar. 2017.
[23] Y. Zhang, J. Liu, H. Yang, and J. Gao, "Direct power control of pulsewidth modulated rectifiers without dc voltage oscillations under unbalanced grid conditions," *IEEE Trans. Ind. Electron.*, vol. 65, no. 10, pp. 7900–7910, Oct. 2018.
[24] Y. Zhang, J. Jiao, and J. Liu, "Direct power control of PWM rectifiers with online inductance identification under unbalanced and distorted network conditions," *IEEE Trans. Power Electron.*, vol. 34, no. 12, pp. 12524–12537, Dec. 2019.
[25] H. Yang, Y. Zhang, J. Liang, J. Gao, P. D. Walker, and N. Zhang, "Sliding-mode observer based voltage-sensorless model predictive power control of PWM rectifier under unbalanced grid conditions," *IEEE Trans. Ind. Electron.*, vol. 65, no. 7, pp. 5550–5560, Jul. 2018.

Tianbao Song was born in Shandong, China, in 1994. He received the B.S. degree from China University of Mining and Technology, Xuzhou, China, in 2017. He is currently working toward the Ph.D. degree with Tianjin University, Tianjin, China, both in electrical engineering.

His current research interests include ac–dc converters for electric vehicles.

Yun Zhang (Senior Member, IEEE) was born in Jiangsu, China, in 1980. He received the B.S. and M.S. degrees from the Harbin University of Science and Technology, Harbin, China, in 2003 and 2006, respectively, and the Ph.D. degree from the Harbin Institute of Technology, Harbin, China, in 2010, all in electrical engineering.

Subsequently, he was with the Tianjin University, Tianjin, China, as a Lecturer with the School of Electrical and Information Engineering, where he is currently a Professor of Power Electronics. From 2016 to 2017, he was an Academic Visitor with the Power Electronics, Machines and Control Group, University of Nottingham, Nottingham, U.K. His current research interests include topologies, modulation, and control strategies of power converters for electric vehicles and microgrids.

Dr. Zhang is an Associate Editor of the *Journal of Power Electronics*.

Fei Gao (Member, IEEE) received the M.Sc. degree from Shanghai Jiao Tong University, Shanghai, China, in 2010, and the Ph.D. degree for his work on control and stability analysis of more electric aircraft electrical power systems from the PEMC Research Group, University of Nottingham, Nottingham, U.K., in 2016, both in electrical engineering.

From 2010 to 2012, he was with Jiangsu Electric Power Research Institute, Nanjing, State Grid Corporation of China. From 2016 to 2019, he was with Energy and Power Group, University of Oxford, U.K. as a Postdoctoral Researcher. Since Jul. 2019, he has been with Shanghai Jiao Tong University as an Associate Professor. His current research interests include modeling, control, power management, and stability of microgrids and more electric transportation systems.

Dr. Gao was the recipient of the European Union Clean Sky Best Ph.D. Award in 2017.

Chengqian Xu was born in Hebei, China, in 1999. He received the B.S. degree in automation from Hebei University of Technology, Tianjin, China, in 2021. He is currently working toward the M.S. degree in control science and Engineering with Tianjin University, Tianjin, China.

His current research interests include data driven and health status assessment for electric vehicles.

Xinshan Zhu (Member, IEEE) received the B.E. and M.E. degrees in automation control from the Harbin Institute of Technology, Harbin, China, in 2000 and 2002, respectively, and the Ph.D. degree in pattern recognition and intelligent systems from the Institute of Automation, Chinese Academy of Sciences, Beijing, China, in 2005.

He is currently an Associate Professor with the School of Electrical and Information Engineering, Tianjin University, Tianjin, China. His research interests include artificial intelligence, image processing, signal processing, and control for electric vehicles.